Non destructive monitoring of the yoghurt fermentation phase by an image analysis of laser-diffraction patterns: Characterization of cow's, goat's and sheep's milk

Samuel Verdú*, José M. Barat, Raúl Grau

Departamento de Tecnología de Alimentos. Universidad Politècnica de València, Spain

ARTICLE INFO

Keywords:
Image analysis
Yogurt fermentation
Monitoring
Spectral phasor
Diffraction pattern
Laser
Milk
Texture

ABSTRACT

Monitoring yogurt fermentation by the image analysis of diffraction patterns generated by the laser-milk interaction was explored. Cow's, goat's and sheep's milks were tested. Destructive physico-chemical analyses were done after capturing images during the processes to study the relationships between data blocks. Information from images was explored by applying a spectral phasor from which regions of interest were determined in each image channel. The histograms of frequencies from each region were extracted, which showed evolution according to textural modifications. Examining the image data by multivariate analyses allowed us to know that the captured variance from the diffraction patterns affected both milk type and texture changes. When regression studies were performed to model the physico-chemical parameters, satisfactory quantifications were obtained (from R^2 = 0.82 to 0.99) for each milk type and for a hybrid model that included them all. This proved that the studied patterns had a common fraction of variance during this processing, independently of milk type.

1. Introduction

The continuous improvement of industrial activities is horizontal motivation that affects the most traditional and most recent processes. Some improvement areas include reducing operation times, energy costs and waste and, in this sense, the food industry does not differ much from others. Improvements in production lines can be generally made by substituting outdated equipment and technologies, making modifications in equipment materials, etc. Modifying and adapting the analysis and control techniques during processes can also lead to major short-term improvements without incurring high economic and time costs (Abdul Halim Lim, Antony, Garza-Reyes, & Arshed, 2015; Lim & Antony, 2016). The most important aspect of this approach is that it quickly collects vast amounts of data from process operations to increase knowledge about it, and to then improve decision making about any modifications required at any time. Most of the devices and techniques used for this purpose operate non destructively (Chen, Zhang, Zhao, & Ouyang, 2013; Ropodi, Ropodi, Panagou, & Nychas, 2016). This implies collecting data without coming into contact with or modifying samples. In the food industry, this research area represents not only optimizing resources for processing, but also major advances in quality/safety control terms from raw material reception to end product storage (Arendse, Fawole, Magwaza, & Opara, 2017).

Some of the techniques accordingly applied are based on spectroscopic determinations (principally within infrared ranges), ultrasounds, electronic tongues, image analyses, and some combinations of them all. Some examples of industrial approach applications are classifying chicken breast fillets (Barbin et al., 2015; Yang et al., 2018), rapidly detecting defects in maize (Sendin, Manley, & Williams, 2017), predicting freshness in tilapia (Shi et al., 2018), continuously monitoring bread dough fermentation (Verdú, Ivorra, Sánchez, Barat, & Grau, 2015), detecting wheat flour adulterations (Verdú et al., 2016), predicting banana properties (Xie, Chu, & He, 2017), determining the antioxidant capacity of aromatically plants (Fuentes et al., 2017), etc. The physico-chemical nature of the food matrix, as well as the specific transformations that take place during processes, delimit the suitability of each technique to measure a given analyte and to then condition features of applications.

In the dairy industry, raw materials also present slight microbiological stability, multiphase composition and different available origins, whose processing control and derived products are susceptible to improvement by such techniques. Some recent reports with satisfactory results have detected melamine and additives in milk powders by hyperspectral imaging (Fu et al., 2014; Mabood et al., 2017),

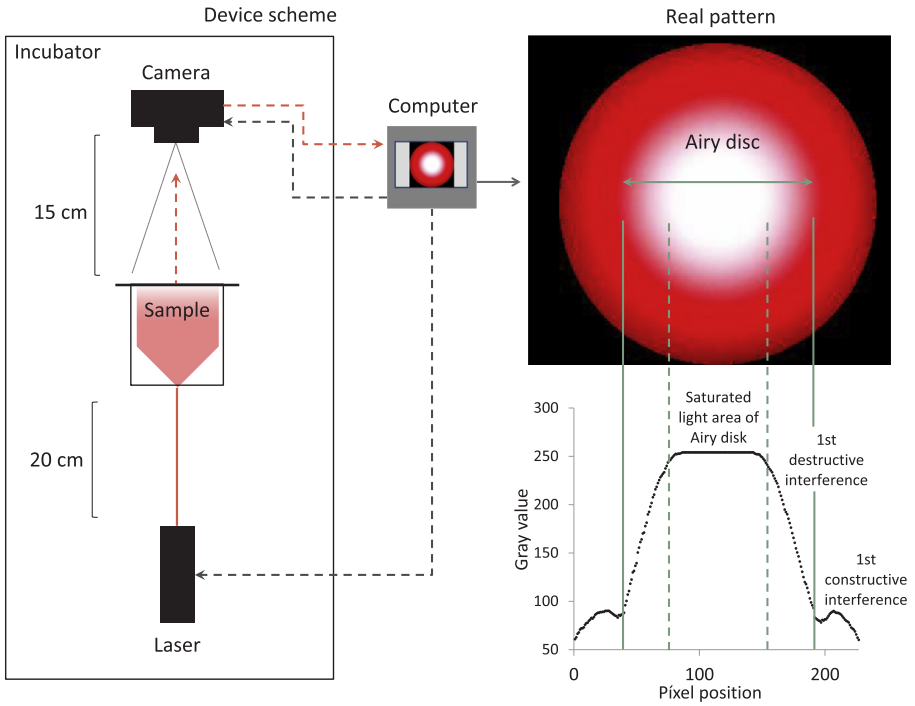

Fig. 1. Scheme of the device to run the experiment, and an image of the real pattern captured during the experiment and its profile in grayscale terms (bottom part). Green lines mark the different pattern zones.

and additive components in powdered milk by NIR imaging (Huang, Min, Duan, Wu, & Li, 2014), etc.

In this sector, yogurt processing has features that make improvements to reduce operation times difficult because bacteriological and biochemical activities are necessary. However, knowledge about fermentation as regards liquid matrix status, phase changes and textural properties could provide valuable information for new developments to be applied to fermentation systems, product formulas and raw material adaptations. The physico-chemical evolution produced during this process makes obtaining continuous and rapid information about the influence of several process variables on the isoelectric point of proteins and gelification kinetics most interesting. Some examples of these variables are the nature of milk, fermentation temperature, microbial starters, texture modifiers, etc. Very few recent reports can be found about non destructive techniques used to monitor yogurt processing. Yogurt fermentation monitoring using electronic tongues (Wei, Zhang, Wang, & Wang, 2017), acoustic impedance methods (Meng, Zhou, Ye, & Liu, 2011) or a combination of NIR and electronic noses (Navrátil, Cimander, & Mandenius, 2004), are some examples. In this research area, our objective is to explore the possibility of monitoring the textural evolution of this food matrix in the fermentation phase of cow's, goat's and sheep's milks by computer vision, and by applying an image analysis to acquire information from generated diffraction patterns that result from the laser-milk interaction during the process.

2. Material and methods

2.1. Raw material and formula

Three different pasteurized milk types were used in this experiment, cow's, goat's and sheep's, which were obtained from local merchants. Milks presented a proximal composition of 3% proteins, 1.5% fat and 4.6% carbohydrates for cow; 3% proteins, 1.5% fat and 4.6% carbohydrates for goat and 5.2% proteins, 1.9% fat and 5.5% carbohydrates for sheep. The other components were 1% (w/w) saccharose (Azucarera Española), and the yogurt starter culture that contains *Streptococcus thermophilus* and *Lactobacillus delbrueckii* subsp. *Bulgaricus* (Chr. Hansen, Horsholm, Denmark).

2.2. Yogurt production

The yogurt formula preparation procedure was based on that of Comunian et al. (2017) with modifications: (1) heat treatment of milks 90 °C/30 min; (2) adding sugar (1%); (3) cooling to 45 °C; (4) adding the yogurt starter culture; (5) dividing the mix into single cylindrical polystyrene packages of 125 g for the fermentation phase at 45 °C to pH ~ 4.6. Two groups of samples from each milk lot were processed under the same conditions: the first was for the image acquisition procedures, and the second was to carry out destructive analyses. Four fermentations from four different lots per milk type were used.

2.3. Texture and pH measurements

pH measurements were taken with a pHmeter BASIC 20+ (CRISON). The method to analyze the product's texture evolution was back strussion (Serra, Trujillo, Guamis, & Ferragut, 2009). A TA-TX2 texture analyzer (Stable Micro Systems, Surrey, UK), equipped with a 25-kilogram load cell, was used in this work. To avoid influencing the matrix structure, samples were analyzed in original packages after cooling to 4 °C using a probe with a disc (∅ = 35 mm) at a constant velocity from 1 mms^{-1} to 50% of sample depth (80 mm). The obtained texture parameters were hardness (maximum positive peak), consistence (area under positive curve/work), adhesive force (maximum negative peak) and adhesiveness (area under negative curve/viscosity index). Measurements were taken every 15 min during the fermentation process using three samples of the second lot.

2.4. Image procedures

2.4.1. Image acquisition

The system was based on capturing the diffraction pattern generated onto the milk/yogurt surface because of the laser light that transmitted

from the lower sample area. The camera (HD cam Logitech C615, CCD, 8 megapixels, Logitech International S.A., Switzerland) was placed vertically in an incubator chamber (KBF720, Binder, Tuttlingen, Germany) 15 cm over the sample surface, which was placed in the middle of the capture field. The laser pointer (650 nm, 50 mW, 3 mm ø) was perpendicularly arranged 20 cm under sample packaging, and was emitted to the bottom-center area (Fig. 1). Three RGB images (3264 × 2448 pixels in the JPEG format) were taken from a single sample every 15 min during each fermentation process. The laser was coordinated with a camera to turn on/off for 1 s per image to avoid influencing sample matrix evolution. Images from four different lots of each milk type were collected.

2.4.2. Image processing

The images obtained during the process showed a typical diffraction pattern, where a maximum intensity peak was generated in the middle, commonly called an Airy disk, along with concentric rings, whose size increased after their intensity reduced. These rings are known as constructive and destructive interferences. An example of an image and its intensity profile on the grayscale are included in Fig. 1. Information from images was obtained using the free software ImageJ following these phases:

1. Split image channels: images were split into their color channels (Red, Green and Blue). This step improves isolating information as well as rejecting noise from the original image. Thus three stacks of images (one per channel) were generated from each fermentation process.
2. Isolate the changing zones of the diffraction patterns: to reject the image zones with no changes during the process, the average of the three images at t0 was subtracted from the rest of the stack. The result was an image group whose histogram features (frequency in pixels of each color value) collected the extent of change compared to t0. These images were called difference images (I^D).
3. Analysis of changing zones' evolution: it was necessary to detect the regions of interest (ROI) from the previous isolated changing zones, which had information according to the fermentation process. Then it was necessary to reject those with noise. A spectral phasor was applied for this step. A brief explanation of the basis of this application is provided in Point 2.4.3.
4. ROI changes quantification and information extraction: The quantification of changes within the selected ROI was based on calculating the image histograms at each sampling time. This operation allows the modifications for each color value (Cv) (from 1 to 255) to be observed to record changes in not only the amount of light, but also in intensity. Data collection was evaluated as a multivariate matrix.

2.4.3. Spectral phasor

Spectral phasor is a method to transform each pixel intensity spectrum into a point on the phasor plot. As each pixel can have a specific spectrum, the position on the phasor plot identifies its spectral shape and peak position. So it is possible to isolate pixels with commonalities during their evolution (the areas delimited by green lines in Fig. 2) and to then detect ROIs. The phasor approach has been previously implemented to analyze fluorescence lifetime (Digman, Caiolfa, Zamai, & Gratton, 2008) and spectral images (Fereidouni, Bader, & Gerritsen, 2012). It is a fast, reliable and easy way to analyze images graphically that requires only low computational power. In our case, the application was to study the spectrum from each pixel which resulted from the changes in the diffraction patterns that took place over time, and to detect those according to texture evolution. The analysis using spectral phasor was carried out with the ImageJ plugin available at http://www.spechron.com/.

2.5. Statistical procedures

The image processing data were processed by applying multivariable statistical procedures to reduce data set dimensionality. To this end, a multivariate unsupervised statistical PCA (principal component analysis) was used to explore the effect of milk nature and fermentation process on the collected information. This method was used to describe and reduce the dimensionality of a large set of quantitative variables (frequency of pixels at each color value of the image channels) of a few new variables, called principal components (PCs), which are the result of the linear combinations of the original variables. Support Vector Machines-Regression (SVM-R) was used to evaluate the relationship between the image data and the physico-chemical properties of milk/yogurt during the process (pH, adhesiveness, adhesive force, consistence and hardness). This method was followed to carry out non linear regressions between both data sets, which were evaluated based on calibration and cross-validation coefficients and root mean square errors (RMSE). The used version was epsilon-support vector regression (ε-SVM), a radial basis function as kernel (RBF kernel), and "*venetian blinds*" as the cross-validation procedure. SVMs are a powerful supervised learning methodology based on the statistical learning theory, which are commonly used for multivariable data sets and the data mining of spectral analyses (Boser, Vapnik, Guyon, & Laboratories, 1992). Procedures were performed with the PLS Toolbox, 6.3 (Eigenvector Research Inc., Wenatchee, Washington, USA), a toolbox extension in the Matlab 7.6 computational environment (The Mathworks, Natick, Massachusetts, USA).

3. Results and discussion

3.1. Texture and pH kinetics during fermentation

The evolutions of the pH and texture parameters measured during the fermentation process are shown in Fig. 2. The pH of milks at t0 was similar. Decreasing pH incremented on the slope around 50 min until 175 min. All three milk types displayed the same behavior and reached ≤4.6 at 210 min. Moreover, texture modifications were not detected within the first 120 min, from which time significant changes were observed in the texture parameters for all three milks at different degrees. Indeed the texture properties of cow's and sheep's milks started to change at the same time (120 min), while goat's milk did so a few minutes later (around 160 min). The process revealed two marked periods: the 1st period, with no texture changes, and the 2nd period, from an inflexion point on the texture parameters until the end of the process. This behavior is the classic milk fermentation process evolution due to milk acidification because of lactic acid production. During the 1st period, pH modification caused the unfolding of whey proteins and the beginning of interactions with one another until pH came close to the isoelectric point (5.2). During the 2nd period, gel forming and rearranging took place due to the precipitation and aggregation of casein structures until pH 4.6 (Lee & Lucey, 2010).

Differences in textural properties were evidenced, which agree with the results reported in other studies (Gursel et al., 2016). Cow's and sheep's milks presented similar results for the hardness and consistence values, while the adhesive force and adhesiveness values were higher for sheep's milk. Goat's milk presented the most different behavior in all the parameters because it presented slight texture changes despite the same pH changes taking place. It is known that the main effect on these features is normally due to differences in the properties of each protein type (Gursel et al., 2016). Gaddour, Najari, & Abdennebi (2013) report that goat's milk yogurt presents poor consistence, hardness and stability compared to the yogurt made from cow's and sheep's milks. According to those reports, the amount of casein micelles and size, and the higher non protein nitrogen content, in goat's than in cow's and sheep milks are all responsible for these differences. However these differences in protein properties could also explain the higher adhesiveness value

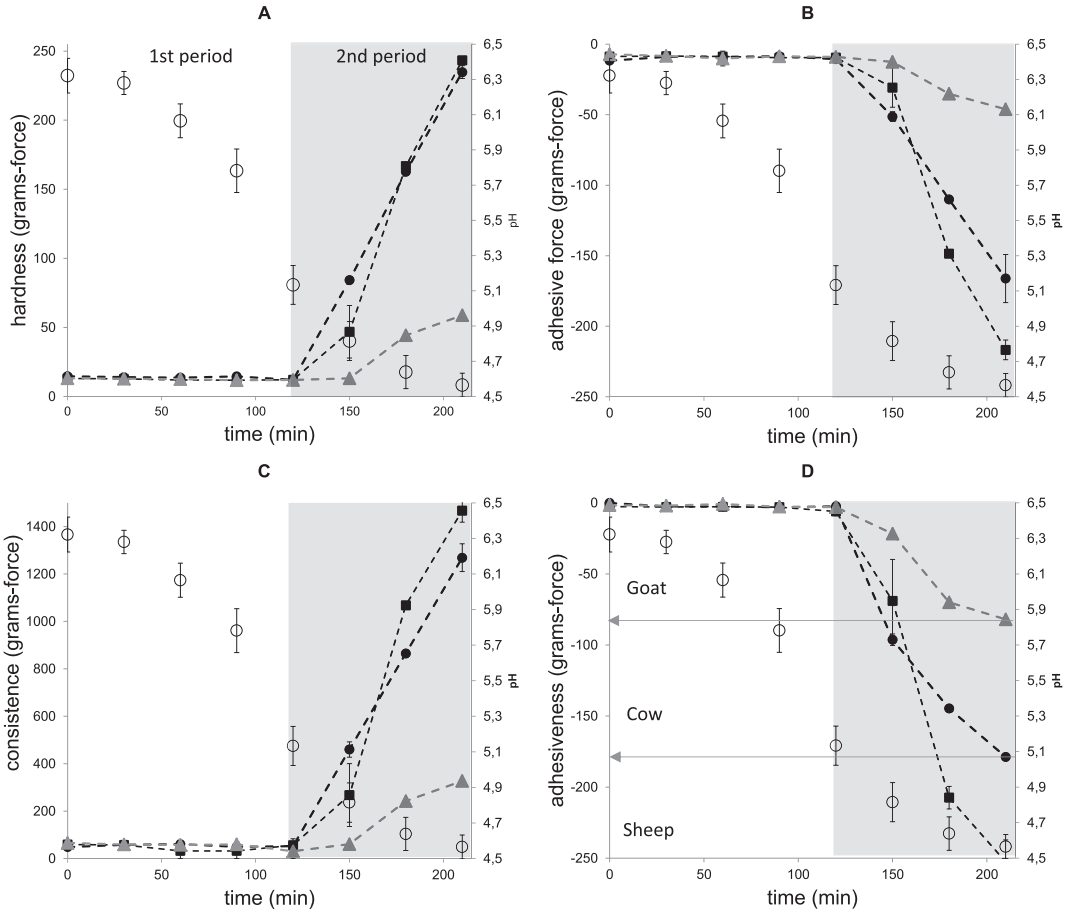

Fig. 2. Kinetics of the pH and texture parameters from the back strussion analysis. A: hardness; B: adhesive force; C: consistence; D: adhesiveness. Circumferences mark the average pH from the three milk types. Dotted lines denote the texture parameters for each milk type: Cow ●; Goat: ▲; Sheep: ■. Water marks mean 2nd period. The arrows in D mean maximum adhesiveness for goat, cow and sheep. Bars indicate standard deviation.

observed for sheep's milk. These behavior patterns were taken as a basis to perform image data processing.

3.2. Evaluating image data

After preparing the images as previously explained, a spectral phasor was applied to obtain the phasor plots of each fermentation process. Since the objective was to determine what image zones collected information about the process (ROIs), the clouds generated inside the phasor plots were analyzed and compared among the milk types (the areas delimited by the green lines in Fig. 2). Fig. 3 illustrates an example of the results for a cow's milk lot. The morphologies of the clouds for each image channel were similar for all three milk types, where commonality was the presence of a large amount of pixels placed relatively far from the center of the plot to form kernels. A considerable pixels fraction dispersed toward the central plot zone. These results allowed the scatter pattern zones to be differentiated, with common evolution observed during the fermentation time from the zones with a non relationship, which could be rejected as noise. The kernel colors inside the image represented the amount of pixels in a given plot zone (similar evolution over time). The established scale went from red (less) to magenta (high). Clouds were explored based on visualizing the pixel kernels in the original images, and representing their evolution with time in intensity terms. The clouds of each channel were divided into three blocks, and the kernel dimensions with more pixels (magenta) (Fig. 2) were taken as a reference. The results showed how channels R and G mainly collected the evolution of the ring that corresponded to the first constructive interference (Fig. 3R, block 1) and the Airy disc (Fig. 3G, block 1) of the observed scatter pattern, respectively, while B collected both zones. In both cases, blocks 1 collected the image area that represented the kernels with the most pixels in each channel. It is noteworthy that the center of the Airy disc was missing in all cases because this zone was the most saturated area in light terms. As this area did not undergo any changes, its information was not available because higher perturbations in the milk matrix were required to modify it.

When the spectra of each block from the clouds were plotted alongside complete cloud evolution with time (Fig. 2, bottom), the excellent contribution of block 1 was observed in both channels R and G. This meant that most of the information fraction inside a complete cloud was collected by the maximum intensity zones of the scatter pattern profile (Airy disc and the first constructive interference ring), collected in image channels R and G. These image zones were those that mainly varied. Although the rest of the image contained part of total variability, it was assumed as noise and was then rejected.

Both R and G presented similar curves, where inflexion points were observed between 100 and 150 min. This behavior could inform about the differentiation of the two previously observed periods during texture evolution (Fig. 2). In this case however, the evolution during the 1st period was also observed, which presented constant behavior regarding the texture analysis parameters. Thus it would appear that the changes that occurred during this time were also recorded by the device. Moreover, channel B displayed behavior, but with no recognizable pattern. It had no specific temporal evolution zone and presented chaotic intensity changes from the entire image.

After detecting the areas from I^D that fitted fermentation evolution, only channels R and G were considered. Those areas considered noise were removed from all the stacks. Information from the ROIs of

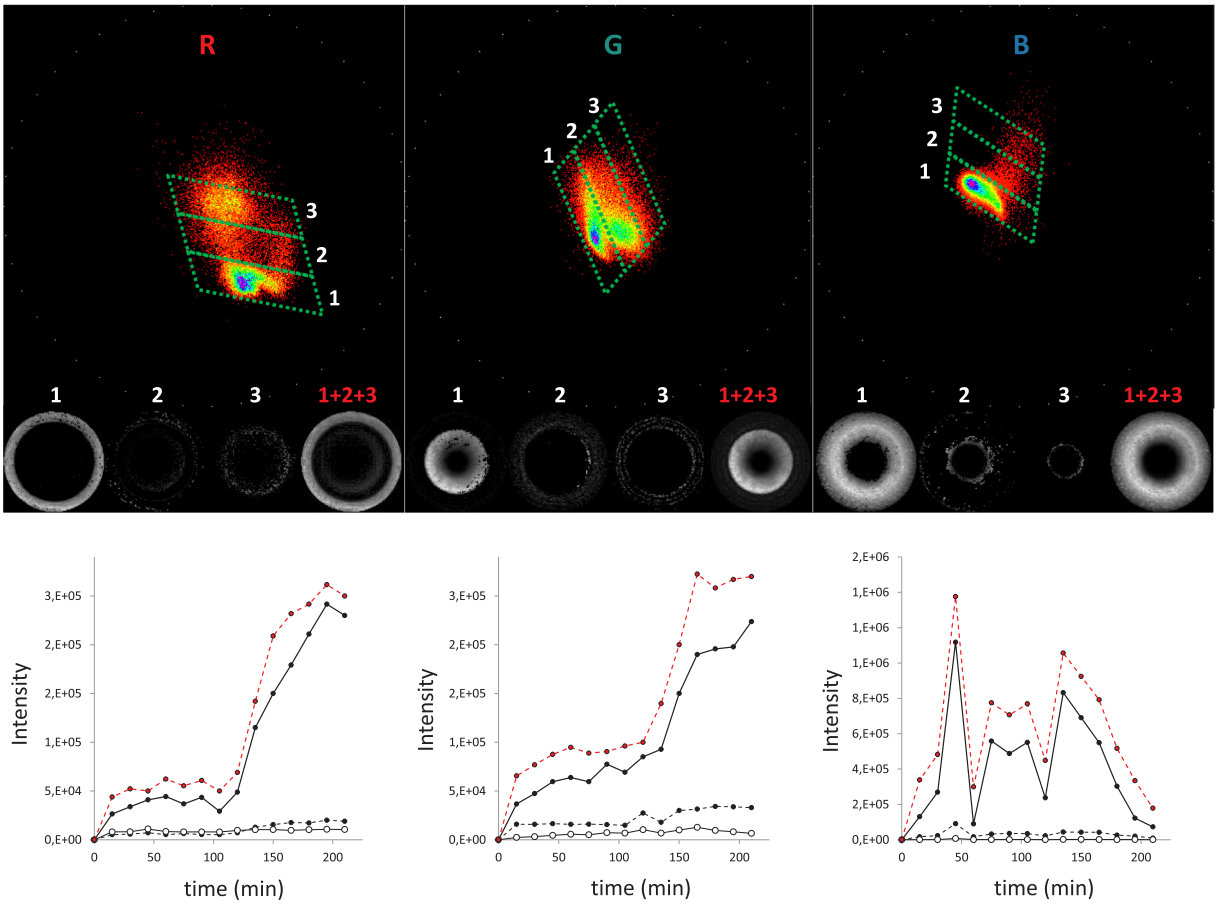

Fig. 3. An example of the spectral phasor analysis to determine the ROIs of a cow's milk lot. Phasor plots for image channels R (red), G (green) and B (blue). The areas delimited by the green dotted rectangles collected different pixel blocks. The bottom numbered images of the phasor plots show the areas of the images that corresponded to each pixel block, and all of them together (1 + 2 + 3). The graphics at the bottom represent the evolution of the intensity of each pixel block (black points: block 1; black points-dotted line: block 2; circumferences: block 3) and the complete pixel cloud (red points-dotted red line: all of them).

channels R and G was collected as explained above. In order to facilitate the visualization of the raw data evolution from the images in terms of the modification of the histogram shape and what color ranges were mainly affected, 3D representations had to be used (based on pixel frequency, color value and time). Fig. 4 shows this representation of a lot example of each milk type. It shows how each color value had its own kinetics with time. Early changes toward minimum values were observed, while maximum values presented most of the changes that occurred during the 2nd fermentation period, when texture changes were recorded. Both channels presented this feature, although channel R was higher. Increasing pixel frequency for a given color value meant that the differences between the pictures of t0 and tn increased; that is, the modification in the light transmittance of the milk matrix was progressive, and then in the diffraction patterns. This effect can be explained with the combination of reduced lactose, lactic acid rising, larger microorganism number, etc. However, protein status was the major influence first on texture and structure properties, and then on the light-matrix interaction. Thus the reduced changes observed in Fig. 2 for goat fitted the slight changes noted during the 2nd period observed in both channels of Fig. 4.

The evolution that took place during the 1st period could be attributed to the protein unfolding processes before the isoelectric point. pH generated changes in these protein structures, which were still too slight to modify texture, but were enough to disrupt the diffraction pattern, principally the dark values that represented most sensitivity as it required fewer light modifications being altered. Moreover, the 2nd period modifications were recorded with all the color values because both gel forming and rearranging were able to disrupt up until the lightest zones of the diffraction patterns. The observed variability fitted the principles that some well-known laboratory methods are based on to take emulsion stability and particle size distribution measurements. These principles have been established by quantifying the light scattering and diffraction features of different kinds of matrices and materials (Agimelen, Mulholland, & Sefcik, 2017; Santos, Calero, Trujillo-Cayado, Garcia, & Muñoz, 2017).

When the generated data matrices were explored by the PCA to reduce dimensionality, differentiation was observed between periods for all the milk types. Fig. 4 depicts the PCA spaces generated per milk type. The results show how periods were separated across PC1 in all cases. The widest separation was for cow's and sheep's milks at the same time as the differences in point dispersion in each period cluster. Once again, the narrowest separation was given for goat's milk compared to the other milk types but, in this case, the dispersion between periods was similar.

The common behavior noted above for the texture evolution periods observed in each milk type data matrix evidenced that the light-milk interactions that took place throughout the process could be recorded during the diffraction patterns images study. In theory, the most widely collected variance could be explained by reorganizations in the milk matrix. However, the effect of milk nature on this common fact was studied because of the differences observed during the physico-chemical characterization. For this purpose, three PCA were performed with all the milk types at a time, but based on different process periods: the first one was done with the entire process data, the second with the data from the 1st period, and the third with the data from the 2nd period. Fig. 5(A and B) shows the results of the first PCA, where the

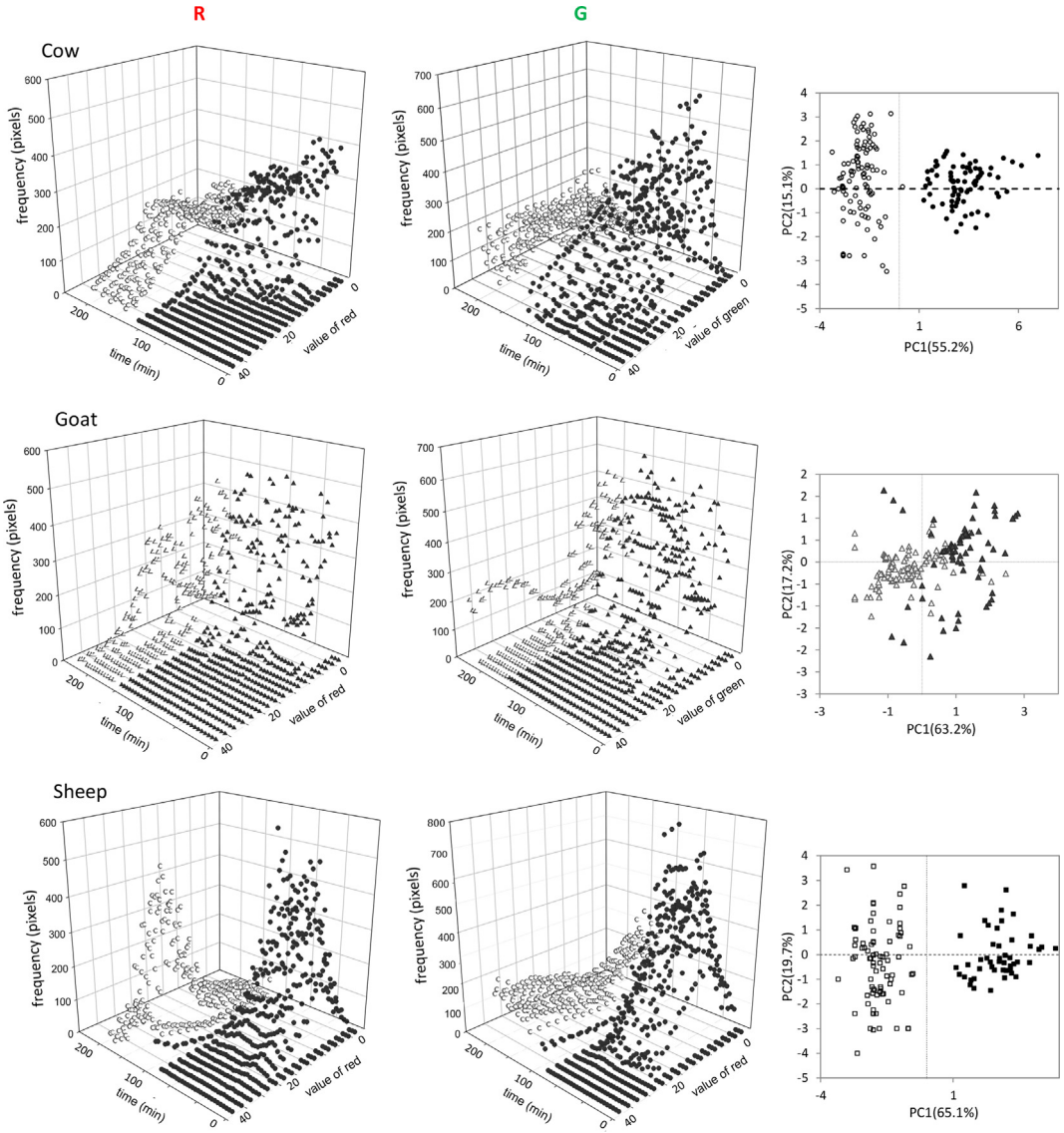

Fig. 4. Detail of the raw image data kinetics. Representation of the raw data from the histograms extracted from the selected ROIs of image channels R (left: external ring/first constructive interference) and G (internal disc/Airy disc) at each time during the fermentation process. Cow ●; Goat: ▲; Sheep: ■. 1st period: dark series; 2nd period: clear series. PCA plots (right) represent the shown raw data as a reduced dimensionality to explore differences between periods.

kinetics of each milk in terms of the PCA scores from the PC1 (61.2% of variance) and PC2 (19.2% of variance) across time are represented. Both PC scores showed evolution with time, but the variance captured by PC1 displayed the most parallelism with that observed previously with the textural parameters (Fig. 2). Major differences in milk behavior from 120 min were once again observed, but they could be also differentiated in this case during the first period. This means that the variance captured by PC1 contains not only the variability caused by textural changes during process, but it was also produced because of milk type. This fact was proved when each period was studied singly in the second and third PCA. Fig. 5C shows the second PCA, done with data from the 1st period, where all the points were arranged as a relatively high dispersion spontaneously, although the three milk clusters were perfectly differentiated. Obviously, the observed dispersion contained the effect of pH during this period. However, the three milk types at t 15 min, when pH had still not significantly lowered, could be differentiated in the center of the plot (red arrows), the zone from which the points evolved in different directions according to milk type. Dispersion reduced when the same study was performed during the 2nd period (third PCA), but the same relative positions were maintained (Fig. 5D). This PCA space showed more defined clusters because differences in milk types increased when texture changes occurred. This clustering happened despite textural changes, whose variance appeared to be collected across PC2. In line with this, cow's and sheep's milks appeared with a similar magnitude for the scores in PC2, while goat's obtained the lowest ones. This result is in accordance with the results of the above-cited physico-chemical analyses, where large differences between sheep's/cow's with goat's milk were obtained. Thus PC2 could collect the variance fraction that corresponded to texture evolution, while PC1 could collect the variance fraction provided by the native differences among all milk types. In any case, we must take into account that part of the variance collected by the diffraction patterns was due to the nature of milk. This result is important for subsequent modeling studies because it could affect the variance produced by the matrix changes with time, and would not thus be common for them all, which could condition the development of a common monitoring model.

Our results evidenced that the device captured the variance produced during the entire fermentation process. This variance could be divided into that provided by milk type and the texture evolution of them all. The acquired information fitted the behavior observed during

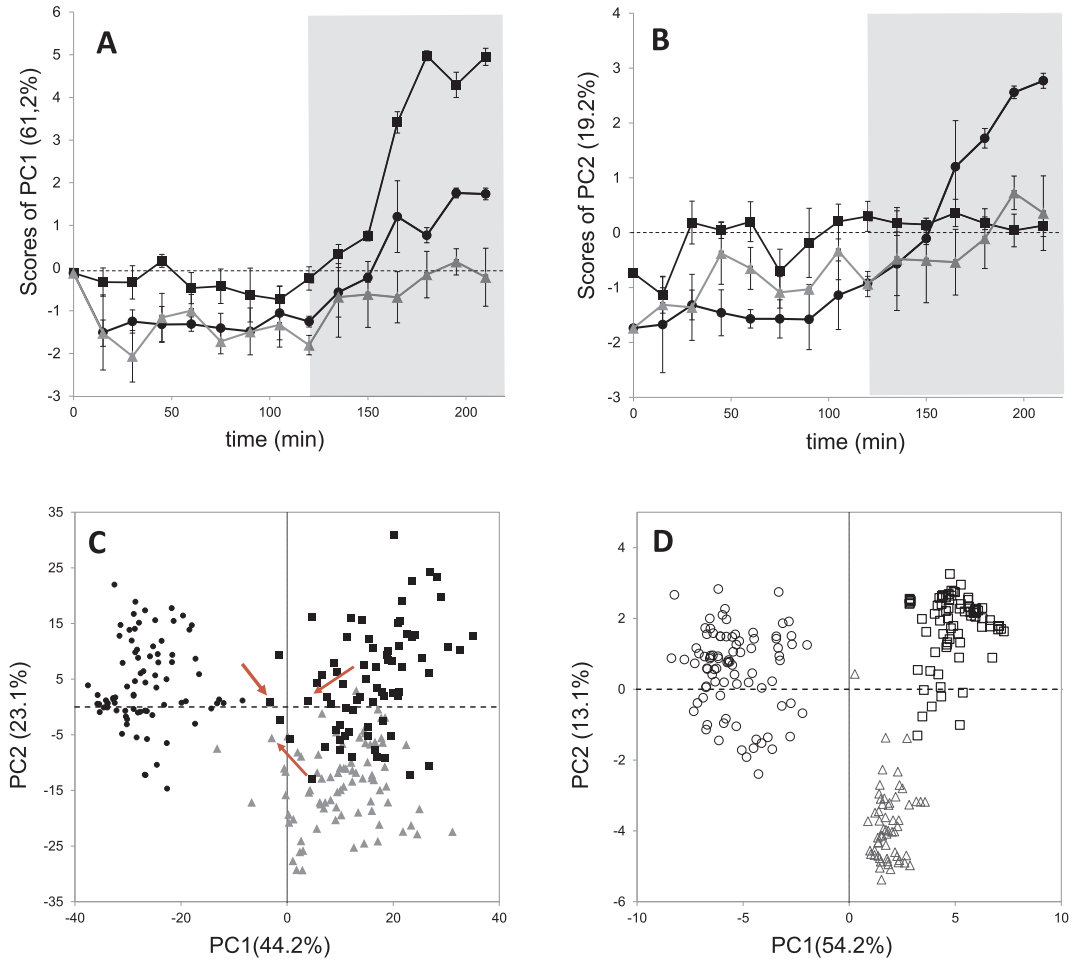

Fig. 5. Study of the milk type effect on the collected data. A and B: Kinetics of the fermentation process in terms of scores from PC1 and PC2 (respectively) of the PCA space generated with the image data of the entire process. C: the PCA space for the image data from the 1st period of the fermentation process; D: the PCA space for the image data from the 2nd period of the fermentation process. Cow ●; Goat: ▲; Sheep: ■. 1st period: filled points; 2nd period: empty points. Red arrows into A mark the samples at t = 15 min.

fermentation in textural terms. Milk type and the changes generated in the matrix led to recognizable diffraction patterns that could be used to characterize and model the process.

3.3. Joint analysis of the physico-chemical and image parameters

Previous qualitative studies have provided knowledge about the properties of the information collected during experiments. However, the quantification of the relationships in the physico-chemical-image data was necessary to determine monitoring capability by generating models. The results of modeling with SVM-R are found in Table 1. The modeling study was done for the 1st period, the 2nd period and the complete process (Cp) for pH, but only for the 2nd period for the texture parameters. These studies were done for each milk type and for all the milk types together in a hybrid model (H_m). This approach allowed us to determine if the collected information had enough common variance loaded to develop hybrid models beyond the differences detected in milk types (Fig. 5).

The coefficients of calibration (R^2 Cal) and cross-validation (R^2 CV) obtained high values, which all fell within the 0.87–0.99 interval, which means that no differences among milk types were observed. The errors calculated for both calibration (RMSEC) and cross-validation (RMSECV) were also similar. These parameters were satisfactory for hybrid modeling (H_m), where the coefficients were good despite collecting all milk type samples.

The results showed the capability of recording the evolution of samples from t0 during the 1st and 2nd periods, despite no textural changes being detected during the 1st period. This can be concluded because of the good correlation with pH evolution during Cp, which means that the registration capability of the biochemical modifications occurred both before and after protein gelation (Fig. 6A). As mentioned above, milk type represented a significant variance fraction in the data, but the fraction of variance provided by the common biochemical phenomenology during the process sufficed to provide good results when hybrid modeling was tested.

This effect was applicable to the texture parameters, where the models provided a good relationship of the image data with all the texture parameter values, independently of milk type. This is observed in Fig. 6B and C. Goat consistency and adhesiveness are placed across the minimum values of both plots because of their reduced texture variation during fermentation. However, cow's and sheep's milk types are arranged across the entire model, and adhesiveness clearly shows this fact. The arrows in Fig. 6C mark the maximum value for goat's (A), cow's (B) and sheep's (C) milks observed in Fig. 2D, and delimit the scope of the points across the plot. Thus from 0 to A, there are points from the three milk types, from B to C there are points from cow's and sheep's milks, while only the points from sheep's milk are placed from C to maximum adhesiveness.

4. Conclusions

The results of our study show the capability of the used device to

Table 1
Results of the *SVM-R* studies. Relationship between the image and physicochemical data.

Physicochemical parameters		Fermentation period	Modelling parameter	Cow	Goat	Sheep	H_m
pH		1st	RMSEC	0.031	0.069	0.039	0.025
			RMSECV	0.103	0.145	0.140	0.189
			R^2 Cal	0.995	0.981	0.988	0.998
			R^2 CV	0.943	0.919	0.853	0.915
		2nd	RMSEC	0.001	0.011	0.011	0.013
			RMSECV	0.054	0.027	0.051	0.065
			R^2 Cal	1.000	0.983	0.994	0.994
			R^2 CV	0.910	0.917	0.856	0.825
		Cp	RMSEC	0.066	0.072	0.065	0.073
			RMSECV	0.121	0.203	0.167	0.179
			R^2 Cal	0.990	0.988	0.988	0.987
			R^2 CV	0.966	0.904	0.926	0.923
Texture	Hardness	2nd	RMSEC	3.197	0.000	3.832	3.479
			RMSECV	9.233	8.784	0.724	1.190
			R^2 Cal	0.980	0.971	0.983	0.951
			R^2 CV	0.922	0.898	0.855	0.842
	Consistency	2nd	RMSEC	0.588	1.055	7.289	4.590
			RMSECV	18.396	49.546	24.567	27.091
			R^2 Cal	0.981	0.992	0.987	0.994
			R^2 CV	0.921	0.820	0.831	0.846
	Adhesive force	2nd	RMSEC	0.438	0.275	7.479	4.713
			RMSECV	1.232	1.785	2.500	1.732
			R^2 Cal	0.950	0.999	0.983	0.993
			R^2 CV	0.923	0.846	0.817	0.886
	Adhesiveness	2nd	RMSEC	3.197	5.400	3.832	3.479
			RMSECV	9.233	8.784	7.200	11.900
			R^2 Cal	0.990	0.991	0.983	0.991
			R^2 CV	0.922	0.898	0.855	0.842

RMSEC: root mean square error of calibration; *RMSECV*: root mean square error of cross-validation; *R^2 Cal*: correlation coefficient of calibration; *R^2 Cal*: correlation coefficient of cross-validation; *H_m*: hybrid modeling.

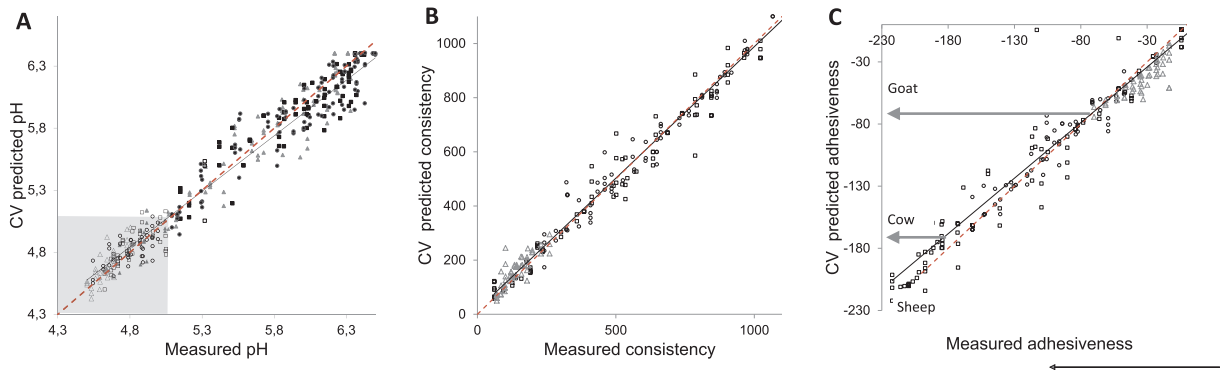

Fig. 6. The observed *vs.* predicted data from the hybrid modeling (H_m) of the complete process *pH* (A) and the 2nd period of consistence (B) and adhesiveness (C). The black line marks tendency lines and the red line denotes line 1:1. The water mark in A marks the 2st period. The arrows in C mean maximum adhesiveness for goat, cow and sheep. Cow ●; Goat: ▲; Sheep: ■. 1st period: filled dots; 2nd period: empty dots.

obtain information about the food matrix in the fermentation phase of yogurt non destructively. The obtained information was isolated from the images after eliminating the zones with no correlation as noise and then finding ROIs according to the measured physico-chemical parameters. Accordingly, the spectral phasor proved an efficient tool to detect ROIs and to reject any other images with irrelevant information. The variance collected by the observed diffraction patterns contributed to both milk type and physico-chemical evolution, which allowed to differentiate between both milk and yogurt types, and the distinct fermentation periods. Despite these differences between milk types, the quantitative modeling of food matrix evolution after and before the isoelectric point of proteins was possible for pH, hardness, consistence, adhesive force, and adhesiveness for each one. Hybrid modeling was also possible with all milk types, which proved that the studied patterns had a common fraction of variance during this processing, independently of milk type. According to these results, future research can involve optimizing collected information by reducing noise during image capture procedures to improve precision, and to test the effect of new yogurt formulas, including additives such as texture modifiers, different probiotic strains, dietetic fiber, etc. The effect of package types and material must also be studied by testing different morphologies and the effect of lids.

References

Abdul Halim Lim, S., Antony, J., Garza-Reyes, J. A., & Arshed, N. (2015). Towards a conceptual roadmap for Statistical Process Control implementation in the food industry. *Trends in Food Science & Technology, 44*(1), 117–129. https://doi.org/10.1016/j.tifs.2015.03.002.

Agimelen, O. S., Mulholland, A. J., & Sefcik, J. (2017). Modelling of artefacts in estimations of particle size of needle-like particles from laser diffraction measurements. *Chemical Engineering Science, 158*, 445–452. https://doi.org/10.1016/j.ces.2016.10.031.

Arendse, E., Fawole, O. A., Magwaza, L. S., & Opara, U. L. (2017). Non-destructive prediction of internal and external quality attributes of fruit with thick rind: A review. *Journal of Food Engineering*. https://doi.org/10.1016/j.jfoodeng.2017.08.009.

Barbin, D. F., Kaminishikawahara, C. M., Soares, A. L., Mizubuti, I. Y., Grespan, M., Shimokomaki, M., & Hirooka, E. Y. (2015). Prediction of chicken quality attributes by near infrared spectroscopy. *Food Chemistry, 168*, 554–560. https://doi.org/10.1016/j.foodchem.2014.07.101.

Boser, E., Vapnik, N., Guyon, I. M., & Laboratories, T. B. (1992). Training algorithm margin for optimal classifiers. *Perception*, 144–152.

Chen, Q., Zhang, C., Zhao, J., & Ouyang, Q. (2013). Recent advances in emerging imaging techniques for non-destructive detection of food quality and safety. *TrAC – Trends in Analytical Chemistry*. https://doi.org/10.1016/j.trac.2013.09.007.

Comunian, T. A., Chaves, I. E., Thomazini, M., Moraes, I. C. F., Ferro-Furtado, R., de Castro, I. A., & Favaro-Trindade, C. S. (2017). Development of functional yogurt containing free and encapsulated echium oil, phytosterol and sinapic acid. *Food Chemistry, 237*, 948–956. https://doi.org/10.1016/j.foodchem.2017.06.071.

Digman, M. A., Caiolfa, V. R., Zamai, M., & Gratton, E. (2008). The phasor approach to fluorescence lifetime imaging analysis. *Biophysical Journal, 94*(2), L14–L16. https://doi.org/10.1529/biophysj.107.120154.

Fereidouni, F., Bader, A. N., & Gerritsen, H. C. (2012). Spectral phasor analysis allows rapid and reliable unmixing of fluorescence microscopy spectral images. *Optics Express, 20*(12), 12729. https://doi.org/10.1364/OE.20.012729.

Fu, X., Kim, M. S., Chao, K., Qin, J., Lim, J., Lee, H., ... Ying, Y. (2014). Detection of melamine in milk powders based on NIR hyperspectral imaging and spectral similarity analyses. *Journal of Food Engineering, 124*, 97–104. https://doi.org/10.1016/j.jfoodeng.2013.09.023.

Fuentes, E., Alcañiz, M., Contat, L., Baldeón, E. O., Barat, J. M., & Grau, R. (2017). Influence of potential pulses amplitude sequence in a voltammetric electronic tongue (VET) applied to assess antioxidant capacity in aliso. *Food Chemistry, 224*, 233–241. https://doi.org/10.1016/j.foodchem.2016.12.076.

Gaddour, A., Najari, S., & Abdennebi, M. (2013). Physicochemical and sensory characteristics of yoghurt produced from goat milk. *Journal of Animal and Veterinary Advances, 12*(24), 1700–1703. https://doi.org/10.3923/javaa.2013.1700.1703.

Gursel, A., Gursoy, A., Anli, E. A. K., Budak, S. O., Aydemir, S., & Durlu-Ozkaya, F. (2016). Role of milk protein–based products in some quality attributes of goat milk yogurt. *Journal of Dairy Science, 99*(4), 2694–2703. https://doi.org/10.3168/jds.2015-10393.

Huang, Y., Min, S., Duan, J., Wu, L., & Li, Q. (2014). Identification of additive components in powdered milk by NIR imaging methods. *Food Chemistry, 145*, 278–283. https://doi.org/10.1016/j.foodchem.2013.06.116.

Lee, W. J., & Lucey, J. A. (2010). Formation and physical properties of yogurt. *Asian-Australasian Journal of Animal Sciences*. https://doi.org/10.5713/ajas.2010.r.05.

Lim, S. A. H., & Antony, J. (2016). Statistical process control readiness in the food industry: Development of a self-assessment tool. *Trends in Food Science & Technology, 58*, 133–139. https://doi.org/10.1016/j.tifs.2016.10.025.

Mabood, F., Jabeen, F., Ahmed, M., Hussain, J., Al Mashaykhi, S. A. A., Al Rubaiey, Z. M. A., ... Manzoor, S. (2017). Development of new NIR-spectroscopy method combined with multivariate analysis for detection of adulteration in camel milk with goat milk. *Food Chemistry, 221*, 746–750. https://doi.org/10.1016/j.foodchem.2016.11.109.

Meng, R. F., Zhou, J. W., Ye, X. Q., & Liu, D. H. (2011). On-line monitoring of yogurt fermentation using acoustic impedance method. *Applied Mechanics and Materials, 101–102*, 737–742. https://doi.org/10.4028/www.scientific.net/AMM.101-102.737.

Navrátil, M., Cimander, C., & Mandenius, C.-F. (2004). On-line multisensor monitoring of Yogurt and Filmjölk fermentations on production scale. *Journal of Agricultural and Food Chemistry, 52*(3), 415–420. https://doi.org/10.1021/jf0304876.

Ropodi, A. I., Ropodi, A. I., Panagou, E. Z., & Nychas, G.-J. E. (2016). Data mining derived from food analyses using non-invasive/non-destructive analytical techniques; determination of food authenticity, quality & safety in tandem with computer science disciplines. *Trends in Food Science & Technology, 50*, 11–25. https://doi.org/10.1016/j.tifs.2016.01.011.

Santos, J., Calero, N., Trujillo-Cayado, L. A., Garcia, M. C., & Muñoz, J. (2017). Assessing differences between Ostwald ripening and coalescence by rheology, laser diffraction and multiple light scattering. *Colloids and Surfaces B: Biointerfaces, 159*, 405–411. https://doi.org/10.1016/j.colsurfb.2017.08.015.

Sendin, K., Manley, M., & Williams, P. J. (2017). Classification of white maize defects with multispectral imaging. *Food Chemistry, 243*(September 2017), 311–318. https://doi.org/10.1016/j.foodchem.2017.09.133.

Serra, M., Trujillo, A. J., Guamis, B., & Ferragut, V. (2009). Evaluation of physical properties during storage of set and stirred yogurts made from ultra-high pressure homogenization-treated milk. *Food Hydrocolloids, 23*(1), 82–91. https://doi.org/10.1016/j.foodhyd.2007.11.015.

Shi, C., Qian, J., Han, S., Fan, B., Yang, X., & Wu, X. (2018). Developing a machine vision system for simultaneous prediction of freshness indicators based on tilapia (*Oreochromis niloticus*) pupil and gill color during storage at 4 °C. *Food Chemistry, 243*(May 2017), 134–140. https://doi.org/10.1016/j.foodchem.2017.09.047.

Verdú, S., Ivorra, E., Sánchez, A. J., Barat, J. M., & Grau, R. (2015). Relationship between fermentation behavior, measured with a 3D vision Structured Light technique, and the internal structure of bread. *Journal of Food Engineering, 146*, 227–233. https://doi.org/10.1016/j.jfoodeng.2014.08.014.

Verdú, S., Vásquez, F., Grau, R., Ivorra, E., Sánchez, A. J., & Barat, J. M. (2016). Detection of adulterations with different grains in wheat products based on the hyperspectral image technique: The specific cases of flour and bread. *Food Control, 62*, 373–380. https://doi.org/10.1016/j.foodcont.2015.11.002.

Wei, Z., Zhang, W., Wang, Y., & Wang, J. (2017). Monitoring the fermentation, postripeness and storage processes of set yogurt using voltammetric electronic tongue. *Journal of Food Engineering, 203*, 41–52. https://doi.org/10.1016/j.jfoodeng.2017.01.022.

Xie, C., Chu, B., & He, Y. (2017). Prediction of banana color and firmness using a novel wavelengths selection method of hyperspectral imaging. *Food Chemistry, 245*(March 2017), 132–140. https://doi.org/10.1016/j.foodchem.2017.10.079.

Yang, Y., Zhuang, H., Yoon, S.-C., Wang, W., Jiang, H., & Jia, B. (2018). Rapid classification of intact chicken breast fillets by predicting principal component score of quality traits with visible/near-Infrared spectroscopy. *Food Chemistry, 244*(17), 184–189. https://doi.org/10.1016/j.foodchem.2017.09.148.